

# Fibroblasts are a site of murine cytomegalovirus lytic replication and Stat1-dependent latent persistence in vivo

---

Sitnik, Katarzyna M.; Krstanović, Fran; Gödecke, Natascha; Rand, Ulfert; Kubsch, Tobias; Maaß, Henrike; Kim, Yeonsu; Brizić, Ilija; Čičin-Šain, Luka

Source / Izvornik: **Nature Communications, 2023, 14**

Journal article, Published version

Rad u časopisu, Objavljena verzija rada (izdavačev PDF)

<https://doi.org/10.1038/s41467-023-38449-x>

Permanent link / Trajna poveznica: <https://um.nsk.hr/um:nbn:hr:184:410870>

Rights / Prava: [Attribution 4.0 International](#)/[Imenovanje 4.0 međunarodna](#)

Download date / Datum preuzimanja: **2025-02-16**



Repository / Repozitorij:

[Repository of the University of Rijeka, Faculty of Medicine - FMRI Repository](#)



# Fibroblasts are a site of murine cytomegalovirus lytic replication and *Stat1*-dependent latent persistence in vivo

Received: 2 July 2022

Accepted: 29 April 2023

Published online: 29 May 2023

 Check for updates

Katarzyna M. Sitnik <sup>1,2,6</sup>✉, Fran Krstanović <sup>3</sup>, Natascha Gödecke <sup>1</sup>, Ulfert Rand <sup>1</sup>, Tobias Kubsch<sup>1</sup>, Henrike Maaß <sup>1</sup>, Yeonsu Kim<sup>1</sup>, Ilija Brizić <sup>3</sup> & Luka Čičin-Šain <sup>1,4,5,6</sup>✉

To date, no herpesvirus has been shown to latently persist in fibroblastic cells. Here, we show that murine cytomegalovirus, a  $\beta$ -herpesvirus, persists for the long term and across organs in PDGFR $\alpha$ -positive fibroblastic cells, with similar or higher genome loads than in the previously known sites of murine cytomegalovirus latency. Whereas murine cytomegalovirus gene transcription in PDGFR $\alpha$ -positive fibroblastic cells is almost completely silenced at 5 months post-infection, these cells give rise to reactivated virus *ex vivo*, arguing that they support latent murine cytomegalovirus infection. Notably, PDGFR $\alpha$ -positive fibroblastic cells also support productive virus replication during primary murine cytomegalovirus infection. Mechanistically, *Stat1*-deficiency promotes lytic infection but abolishes latent persistence of murine cytomegalovirus in PDGFR $\alpha$ -positive fibroblastic cells *in vivo*. In sum, fibroblastic cells have a dual role as a site of lytic murine cytomegalovirus replication and a reservoir of latent murine cytomegalovirus *in vivo* and STAT1 is required for murine cytomegalovirus latent persistence *in vivo*.

Murine cytomegalovirus (MCMV) belongs to the genus *Murine cytomegalovirus* in the subfamily *Betaherpesvirinae*. It is most closely related to the primate-infecting viruses of the genus *Cytomegalovirus*, comprising human cytomegalovirus (HCMV). Together, cytomegaloviruses are characterized by large DNA genomes (>200 kb), induction of cytomegaly in infected cells and strict species tropism<sup>1</sup>. As for all herpesviruses, the life cycle of cytomegaloviruses comprises both lytic (productive) and latent (non-productive) infection, the latter underpinning their ability to persist for life in their respective hosts. During lytic infection, the cytomegalovirus genome is transcribed to express high levels of immediate-early (IE), early (E) and late (L) viral gene products, added in a temporal sequence, that carry the virus through the phases of the genome replication and

virion assembly, culminating in the release of infectious virions and cell lysis. By contrast, during latent infection, cytomegalovirus genomic DNA persists in the cell nucleus, but the viral progeny is not produced. Viral gene transcription in latency is considerably silenced and cytomegalovirus major IE promoter is associated with histones bearing repressive post-translational marks<sup>2,3</sup>. Under appropriate conditions, the virus productive cycle is reactivated, leading to the genesis of new infectious progeny. A formal criterium of latency is the appearance of the infectious virus upon, but not prior to, cocultivation of the population of interest with cells permissive to lytic infection. *In vivo*, lytic cytomegalovirus infection prevails for some time following virus inoculation, enabling viral amplification and spread, but in immunocompetent hosts it is eventually extinguished,

<sup>1</sup>Department of Viral Immunology, Helmholtz Centre for Infection Research, 38124 Braunschweig, Germany. <sup>2</sup>Department of Biomedical Sciences, University of Veterinary Medicine Vienna, 1210 Vienna, Austria. <sup>3</sup>Center for Proteomics, Faculty of Medicine, University of Rijeka, 51000 Rijeka, Croatia. <sup>4</sup>Centre for Individualized Infection Medicine, a joint venture of HZI and MHH, 30625 Hannover, Germany. <sup>5</sup>German Centre for Infection Research (DZIF), Hannover-Braunschweig site, 38124 Braunschweig, Germany. <sup>6</sup>These authors contributed equally: Katarzyna M. Sitnik, Luka Čičin-Šain.

✉ e-mail: [Katarzyna.Sitnik@vetmeduni.ac.at](mailto:Katarzyna.Sitnik@vetmeduni.ac.at); [luka.cicin-sain@helmholtz-hzi.de](mailto:luka.cicin-sain@helmholtz-hzi.de)

after which a life-long phase of in vivo latency ensues when only latent virus can be detected<sup>4</sup>.

Herpesviruses are recognized for using distinct cell types as sites of lytic replication and latent persistence<sup>5</sup>. In line with this, myeloid progenitors and monocytes are well-characterised sites of HCMV latency<sup>6</sup>. Latent infection of these cell types by MCMV is less clear, due to conflicting results in studies<sup>7,8</sup> and remains a controversial topic. On the other hand, and somewhat curiously for a herpesvirus, latent MCMV was found to reside during in vivo latency in liver endothelial cells<sup>8</sup> and peritoneal macrophages<sup>9,10</sup>, which represent cell types that are permissive to lytic MCMV infection<sup>9,11</sup>. Fibroblasts are also well-known to support lytic MCMV replication and are commonly used to grow virus stocks<sup>12</sup>. Interestingly, experiments of Mercer et al.<sup>13</sup> and Pomeroy et al.<sup>14</sup> performed more than 30 years ago, demonstrated enrichment for MCMV genomes and virus reactivation from stroma-enriched spleen fragments, while essentially excluding the contribution of hematopoietic cells. The authors proposed that splenic fibroblasts were involved but could not prove it due to the lack of available methods for splenic fibroblast purification. Notably, the notion about latency in fibroblastic cells has since not been investigated for MCMV or any other herpesvirus, and remains unconfirmed.

Like other viral infections, MCMV is crucially controlled by the host's response to interferons (IFNs)<sup>15</sup>, which signal through signal transducer and activator of transcription 1 (STAT1)<sup>16</sup>. Mice deficient for *Stat1* or otherwise rendered unresponsive to IFNs succumb within a few days to infection with only a few hundred plaque forming units (PFU) of MCMV<sup>17,18</sup>. Besides orchestrating antiviral immunity through effects on the functions of the cells of the immune system, IFNs directly inhibit productive MCMV growth by elevating cell-intrinsic antiviral activity<sup>15,19,20</sup>. Notably, IFN treatment inhibits the activity of MCMV major IE promoter, which controls the initiation of the lytic cycle<sup>20</sup>. We have shown that MCMV infection in permissive cells infected at low multiplicity of infection (MOI) in the presence of IFN is transiently repressed until IFN is removed. This reversible state satisfied the formal definition of latency, where MCMV genomes are maintained in absence of replicating virus, but the virus has the capacity to reactivate<sup>20</sup>. However, it remained unclear if similar phenomena may be observed in a long-term in vivo model of cytomegalovirus latency.

In this study, using state-of-the-art methods for the purification of tissue-resident subsets from mouse organs, we comprehensively mapped the cellular sites of MCMV genome persistence during latency in vivo. Our study unravels that MCMV commonly persists in PDGFR $\alpha$ <sup>+</sup> fibroblastic cells for the long term, in a state that fulfils all the formal criteria of latent infection. We further show that PDGFR $\alpha$ <sup>+</sup> fibroblastic cells are simultaneously permissive to lytic MCMV infection and have a role in viral reproduction during the acute phase of in vivo infection. Finally, we identify a physiological role of STAT1 in enabling latent persistence of MCMV in fibroblastic cells in vivo whilst concurrently inhibiting their lytic infection with the virus.

## Results

### PDGFR $\alpha$ <sup>+</sup> fibroblastic cells carry MCMV genomes during latent MCMV infection in vivo

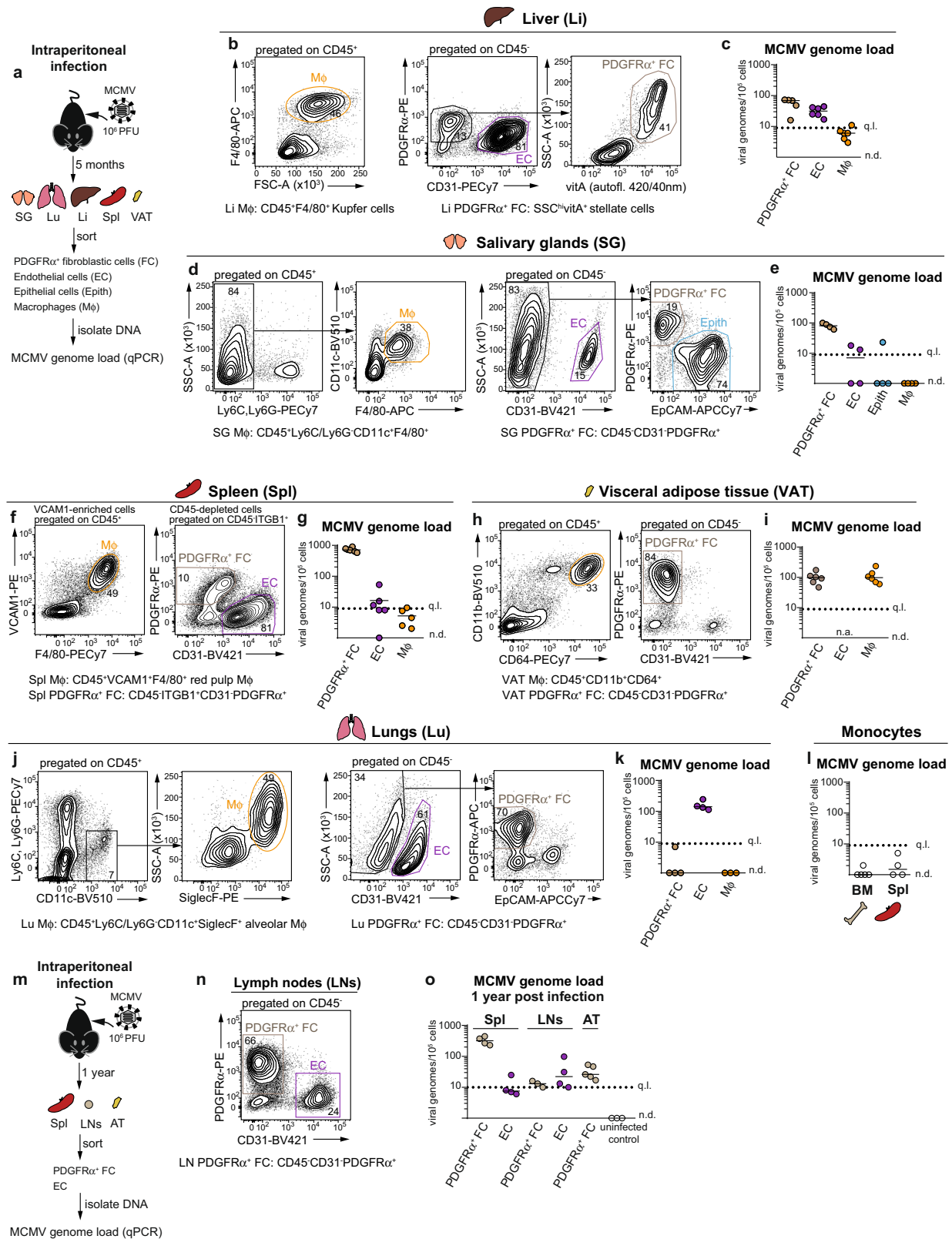
To address whether fibroblastic cells might be a site of MCMV latent persistence in vivo, we initially performed a comprehensive characterisation of the distribution of MCMV genomes in tissue-resident cells across mouse organs during latency in vivo. Specifically, we determined the number of viral genome copies per 100,000 cells (henceforth referred to as MCMV genome load) in FACS-sorted fibroblastic-, endothelial-, epithelial- and tissue-resident macrophage populations from the liver, salivary glands (SG), spleen, visceral adipose tissue (VAT) and lungs of mice latently infected via intraperitoneal route (Fig. 1, for pre-gating schemes for all cell populations see Supplementary Fig. 1a). Intraperitoneal administration of MCMV is the most widely used MCMV infection model that results in infection of

multiple organs due to virus systemic spread in the acute phase of infection<sup>21,22</sup>. Populations of tissue-resident macrophages (M $\phi$ ), such as F4/80<sup>+</sup>CD11c<sup>+</sup> SG M $\phi$ , lung alveolar M $\phi$ , liver Kupfer cells, spleen red pulp M $\phi$  and VAT M $\phi$  were identified using organ-specific gating strategies<sup>23–25</sup>. Endothelial cells (EC) were identified as CD45<sup>+</sup>PDGFR $\alpha$ CD31<sup>+</sup> cells and were shown to co-express CD146 in the liver (Supplementary Fig. 1b). Of note, EC from VAT were not analysed as they could not be isolated in sufficient numbers. PDGFR $\alpha$ <sup>+</sup> fibroblastic cells (PDGFR $\alpha$ <sup>+</sup> FC) were identified as CD45<sup>+</sup>CD31<sup>+</sup>PDGFR $\alpha$ <sup>+</sup> cells in VAT<sup>26</sup>, CD45<sup>+</sup>CD31<sup>+</sup>EpCAM<sup>+</sup>PDGFR $\alpha$ <sup>+</sup> cells in the lungs<sup>27</sup> and SG<sup>28</sup>; and as CD45<sup>+</sup>CD31<sup>+</sup>ITGB1<sup>+</sup>PDGFR $\alpha$ <sup>+</sup> cells in the spleen<sup>29</sup>. In the liver we focused on a defined CD45<sup>+</sup>CD31<sup>+</sup>EpCAM<sup>+</sup>PDGFR $\alpha$ <sup>+</sup> FC subset, vitamin A<sup>+</sup> liver stellate cells<sup>30,31</sup>. We chose to focus on FC that express PDGFR $\alpha$  since they are relatively well-defined across mouse organs<sup>32</sup>. To quantify MCMV genome load, genomic DNA isolated from sorted cell subsets was used as input in a quantitative PCR assay with primers specific to viral gB gene and to mouse *Pthrp* gene. Absolute quantification was performed using serial dilutions of a plasmid carrying both gB and *Pthrp* sequences, according to a previously described method<sup>33</sup>, with a quantitation limit of 10 copies of the plasmid standard in a single qPCR reaction (Supplementary Fig. 1c). Strikingly, PDGFR $\alpha$ <sup>+</sup> FC carried the highest viral genome load across multiple tissues, in the liver (ca 2-fold), in SG (ca 10-fold) and most substantially, in the spleen (ca 100-fold) (Fig. 1b–i). Only in the lungs were MCMV genomes absent from PDGFR $\alpha$ <sup>+</sup> FC (Fig. 1j, k). EC carried MCMV genomes in liver and lungs, which is consistent with previous reports<sup>5,34</sup>, but their MCMV genome content appeared lower in the spleen and was barely detectable in the SG (Fig. 1b–k). MCMV genomes were detected in VAT M $\phi$  at levels similar to PDGFR $\alpha$ <sup>+</sup> FC from the same site, but were absent or barely detectable in M $\phi$  from other organs (Fig. 1b–k). Next, to compare the viral genome load in PDGFR $\alpha$ <sup>+</sup> FC to that of circulating myeloid cells, we analysed monocytes isolated from the bone marrow (BM) or the spleen of latently infected mice. We detected <10 copies of MCMV genomes (Fig. 1l), which is 10–100-fold lower than carried by PDGFR $\alpha$ <sup>+</sup> FC in all organs tested except the lungs. Importantly, MCMV genomes persisted in PDGFR $\alpha$ <sup>+</sup> FC even 1 year after infection, as shown for PDGFR $\alpha$ <sup>+</sup> FC from the spleen, lymph nodes (LNs)<sup>35</sup> and VAT (Fig. 1m–o). Together, these results reveal that MCMV genomes are commonly present in PDGFR $\alpha$ <sup>+</sup> FC of multiple organs during MCMV latency in vivo.

### The route of infection determines the load of MCMV genomes in PDGFR $\alpha$ <sup>+</sup> FC of latently infected lungs

Our finding that following intraperitoneal infection MCMV genomes persist in PDGFR $\alpha$ <sup>+</sup> FC in all organs except the lungs was intriguing. We previously compared mucosal routes of infection, such as intranasal or intragastric, with intraperitoneal infection and observed that intranasal infection is the more efficient route of MCMV infection for the lungs<sup>36</sup>. Nevertheless, intranasal infection results in a more restricted pattern of virus spread than the intraperitoneal infection route, involving only the lungs and SG, which was in line with a previous report<sup>37</sup>. Notably, the cellular sites of MCMV latency after intranasal infection, which is thought to better model the natural MCMV infection<sup>38</sup>, are yet to be investigated. Therefore, we next determined MCMV genome load in PDGFR $\alpha$ <sup>+</sup> FC, EC as well as epithelial cells and M $\phi$  from the lungs and SG of mice latently infected via intranasal route (Fig. 2a).

Notably, PDGFR $\alpha$ <sup>+</sup> FC carried the highest MCMV genome load of all tested subsets in both lungs and SG of mice infected intranasally (Fig. 2b, c). Thus, distinct routes of infection result in differences in MCMV genome distribution in PDGFR $\alpha$ <sup>+</sup> FC in the lungs. Whether this is due to putative differences in the exposure/accessibility of PDGFR $\alpha$ <sup>+</sup> FC to the virus during acute infection and/or putative differential effects on virus persistence in PDGFR $\alpha$ <sup>+</sup> FC remains to be clarified in future studies.



**Differences in MCMV genome load between PDGFR $\alpha$ <sup>+</sup> and PDGFR $\alpha$ <sup>-</sup> FC during latency in vivo**

Next, we asked whether other populations of FC, which do not express PDGFR $\alpha$ , carried similar MCMV genome load in latently infected mice as PDGFR $\alpha$ <sup>+</sup> FC. To this end, we determined MCMV genome load in distinct subsets of FC from the lungs of mice latently infected either intraperitoneally or intranasally (Fig. 3a). The CD45<sup>+</sup>CD31<sup>+</sup>EpCAM<sup>+</sup> cell

fraction from the lungs (for pre-gating see Supplementary Fig. 2a) consisted of two discrete compartments, a major subset of PDGFR $\alpha$ <sup>+</sup> FC, which is known to comprise alveolar, peribronchial and adventitial fibroblasts<sup>27</sup>, and a minor FC population that lacked PDGFR $\alpha$  but expressed PDGFR $\beta$ , hereafter termed PDGFR $\alpha$ <sup>-</sup>PDGFR $\beta$ <sup>+</sup> FC (Fig. 3b). The majority of PDGFR $\alpha$ <sup>-</sup>PDGFR $\beta$ <sup>+</sup> FC expressed CD146 (Supplementary Fig. 2b), fitting with the universal phenotype of mural cells<sup>39</sup>.



**Fig. 1 | PDGFR $\alpha$  fibroblastic cells carry MCMV genomes during latent MCMV infection in vivo.** Analysis of MCMV genome load in indicated cell subsets purified from mice latently infected with MCMV administered intraperitoneally (a–l), 5 months or (m–o), 1 year prior. **a** Experimental design for (b–l). SG submandibular salivary glands, Li liver, Spl spleen, VAT visceral adipose tissue, Lu lungs, BM bone marrow. **m** Experimental design for (n–o). Lymph nodes (LNs) represent pooled inguinal, brachial, axillary, cervical and mesenteric LNs. **b, d, f, h, j, n** Gating strategy for sorting of the indicated cell subsets. Numbers are percentage of cells in the indicated gates. **c, e, g, i, k, l** Number of virus genomes per 100,000 cells 5 months post-infection. Horizontal lines depict median from  $n = 3$  (Lu M $\phi$ ),  $n = 4$  (SG FC, SG EC, SG M $\phi$ , Lu FC, Lu EC, Spl Monocytes),  $n = 5$  (Li FC, Spl M $\phi$ , BM Monocytes) or

$n = 6$  (Li FC, Li EC, Spl FC, Spl EC, VAT FC, VAT M $\phi$ ) biologically independent samples (depicted as symbols) examined over two independent experiments. Biological replicates represent cells sorted from pooled preparations from 1 to 2 (Li, Lu), 2 (SG, VAT, Monocytes) or 4 (Spl) mice. Sorting was done either from 1 organ (VAT, Spl) or simultaneously from two organs (SG and Lu; Li and BM) per biological replicate. **o** Number of virus genomes per 100,000 cells 1 year post-infection. Horizontal lines depict median from  $n = 3$  (LN FC),  $n = 4$  (Spl FC, Spl EC, LN EC) or  $n = 5$  (VAT FC) biologically independent samples (depicted as symbols) examined over two independent experiments. Biological replicates represent cells sorted from pooled preparations from 2 (VAT) or 4 (Spl, LNs) mice. q.l. quantification limit, n.d. not detected, n.a. not analysed. Source data are provided as a Source Data file.

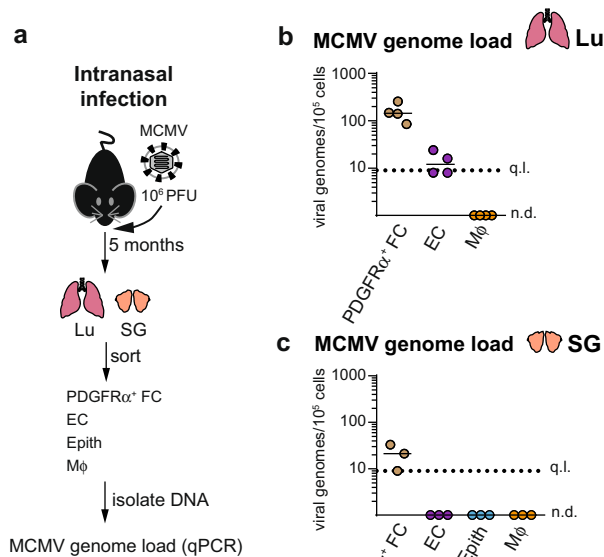


**Fig. 2 | The route of infection determines the MCMV genome content of PDGFR $\alpha$  FC in latently infected lungs.** Analysis of MCMV genome load in indicated cell subsets purified from mice latently infected with MCMV administered intranasally 5 months prior. **a** Experimental design. **b, c** Number of virus genomes per 100,000 cells. Horizontal lines depict median from  $n = 3$  (SG) or  $n = 4$  (Lu) biologically independent samples (depicted as symbols) examined over two independent experiments. SG and Lu subsets were simultaneously obtained from 1 to 2 mice per replicate. q.l. quantification limit, n.d. not detected. Source data are provided as a Source Data file.

Following intraperitoneal infection, which as shown in Fig. 1k results in the preferential distribution of MCMV genomes to EC, both PDGFR $\alpha$ + FC and PDGFR $\alpha$ - PDGFR $\beta$ + FC were a minor source of MCMV genomes with the load of <10 viral genome copies per 100,000 cells (Fig. 3c). Following intranasal infection, which as shown in Fig. 2b results in the preferential distribution of MCMV genomes to PDGFR $\alpha$ + FC, viral genomes were robustly detected in both FC subsets but the genome load in PDGFR $\alpha$ - PDGFR $\beta$ + FC was a 3-fold lower compared to PDGFR $\alpha$ + FC (one-way ANOVA F (2,9) with Dunnett's multiple comparisons test,  $p = 0.0007$ , 95% confidence interval (CI) of the difference = -156.4 to -56.57) (Fig. 3d). We also mapped the distribution of MCMV genomes during latency in the subpopulations of FC from the spleens of mice infected intraperitoneally (Fig. 3e). We fractionated CD45<sup>-</sup> CD31<sup>-</sup> ITGBI<sup>+</sup> splenic FC<sup>29</sup> (for pre-gating see Supplementary Fig. 2c) into Ly6C<sup>+</sup> red pulp FC, BST-1<sup>-</sup> white pulp FC, and BST-1<sup>-</sup> Ly6C<sup>-</sup> FC (hereafter termed, other FC), which are mainly composed of CD146<sup>+</sup> mural cells<sup>29</sup>. As shown in Fig. 3f, Ly6C<sup>+</sup> red pulp FC uniformly expressed high levels of PDGFR $\alpha$ , BST-1<sup>-</sup> white pulp FC contained a minor fraction of PDGFR $\alpha$  cells while other FC consisted mainly of

PDGFR $\alpha$  cells. Notably, MCMV genome load was nearly 10-fold higher in Ly6C<sup>+</sup> red pulp FC compared to BST-1<sup>-</sup> white pulp FC (unpaired *t*-test, degrees of freedom = 6,  $p = 0.0001$ , 95% CI of the difference = 542.5 to 783.5) and to other FC (Fig. 3g). In sum, MCMV genome load in PDGFR $\alpha$ + FC in latently infected lungs and spleen is higher than in PDGFR $\alpha$ - FC in these organs.

### Silenced and stochastic viral gene transcription in PDGFR $\alpha$ + FC from latently infected mice

Next, we investigated if PDGFR $\alpha$ + FC that carried viral genomes during MCMV latency in vivo fulfilled the formal criteria of latent infection. We first asked whether viral gene expression in PDGFR $\alpha$ + FC from latently infected mice was consistent with a putative ongoing lytic viral cycle. To this aim, we measured the expression of viral transcripts from the immediate-early (*ie1/ie3*), early (*M38*) or late (*M48/SCP*) phase of the lytic infection in RNA isolated from PDGFR $\alpha$ + FC from latently infected mice by RT-qPCR (Table 1). We analysed PDGFR $\alpha$ + FC from various organs and conditions in which they were shown to carry MCMV genomes (Figs. 1 and 2), such as the spleen, VAT, SG and liver of mice infected intraperitoneally, and from PDGFR $\alpha$ + FC from the lungs of mice infected intranasally. PDGFR $\alpha$ + FC from the lungs of mice infected intraperitoneally, which are devoid of MCMV genomes (Fig. 1k), were used as a negative control. Liver EC and VAT M $\phi$  from mice infected via intraperitoneal route were also included. Following reverse transcription, copies of cDNA representing each transcript were quantified using serial dilutions of MCMV-BAC<sup>33</sup>, with a quantitation limit of 10 copies of the BAC standard in a single qPCR reaction (Supplementary Fig. 3). Although we used primer pairs that did not distinguish between viral DNA and RNA, our assay specifically detected viral RNA, since no positive signals were obtained when the same RNA samples were processed with the omission of reverse-transcriptase (Supplementary Table 1). To ascertain that comparable amounts of cDNA were used, we standardized our readouts on mouse *Gapdh* expression in all samples. The number of cells corresponding to the cDNA input used per qPCR reaction was estimated for each sample and was in the range of 5,000-15,000 cells (Table 1). Overall, expression of viral mRNAs was detected only sporadically and as no more than a few hundred of copies (Table 1). Specifically, *ie1/ie3* expression was detected in 8, *M38* in 2 and *M48/SCP* in 1 out of 18 tested PDGFR $\alpha$ + FC samples, but none of the samples expressed all three viral genes (Table 1). This transcriptional profile is inconsistent with lytic infection while it fits with the pattern of viral transcription in latently infected lungs described recently by Griessl et al., which was found to be intermittent and stochastic<sup>34</sup>. *ie1/ie3* expression was detected in 1 out of 3 tested liver EC samples and in 1 out of 3 tested VAT M $\phi$  samples, indicating that viral transcription is also silenced in EC and M $\phi$  carrying MCMV genomes during latency in vivo. In sum, the profile of viral gene expression in PDGFR $\alpha$ + FC from latently infected mice is at odds with persistent lytic infection.

### PDGFR $\alpha$ + FC carry latent MCMV in vivo

To test for functional criteria of latency, we next determined if MCMV can reactivate from PDGFR $\alpha$ + FC purified from latently infected mice.

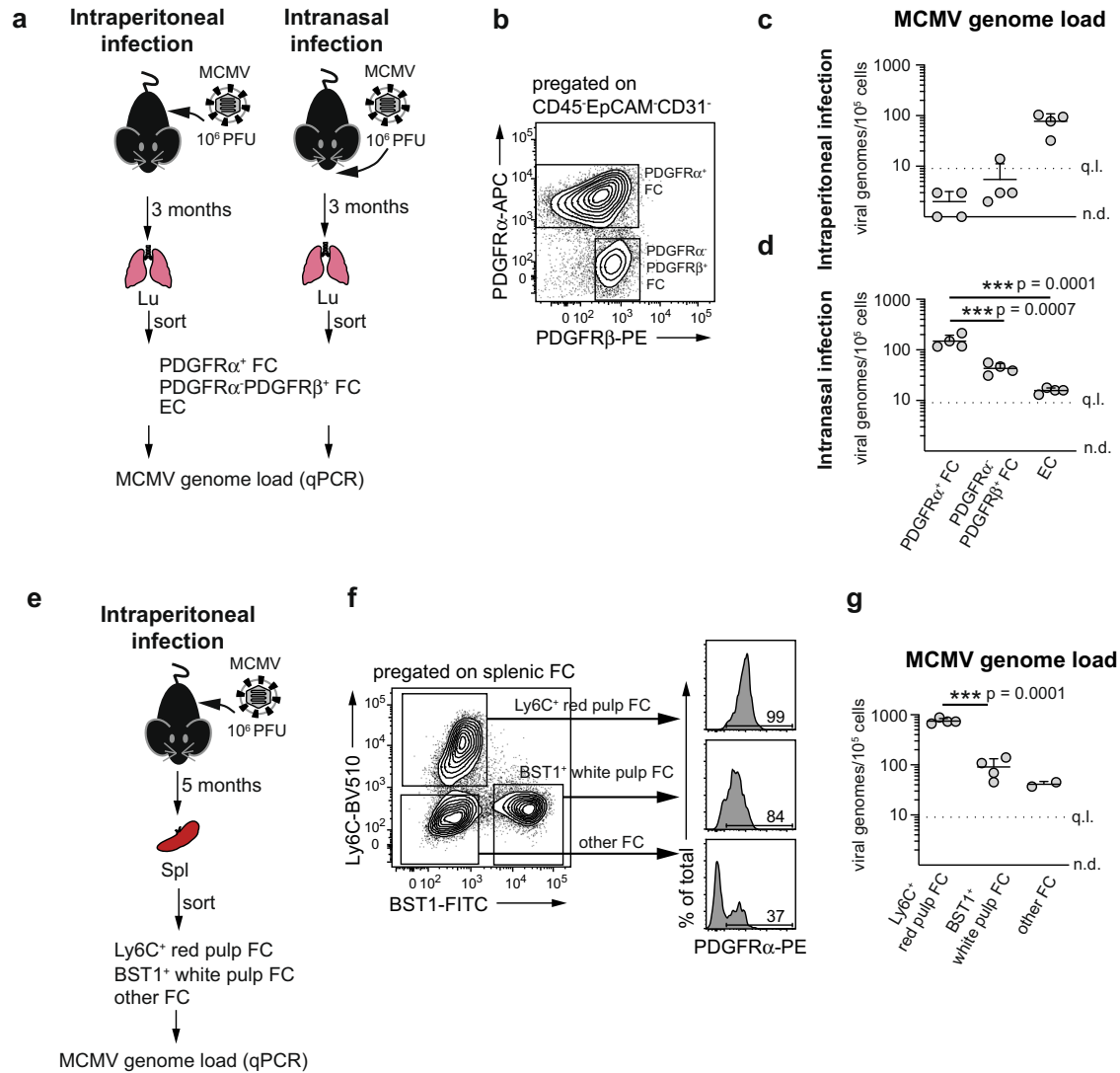


**Fig. 3 | Differences in MCMV genome load between PDGFR $\alpha^+$  and PDGFR $\alpha^-$  FC during latency in vivo.** Analysis of MCMV genome load in indicated FC subsets purified from the lungs of mice latently infected with MCMV administered intraperitoneally or intranasally (a–d), or the spleen of mice latently infected with MCMV administered intraperitoneally (e–g). **a** Experimental design for (b–d). **e** Experimental design for (f, g). **b, f** Gating strategy for sorting of the indicated cell subsets. **c, d, g** Number of virus genomes per 100,000 cells. **c, d** Horizontal line depicts the arithmetic mean  $\pm$  SD from  $n = 4$  biologically independent samples (depicted as symbols) examined over two independent experiments. Biological

replicates represent cells sorted from pooled preparations from two mice. \*\*\* $p$ -value  $< 0.001$  (exact values indicated in the figure), one-way ANOVA with Dunnett’s multiple comparisons test. **g** Horizontal line depicts the arithmetic mean  $\pm$  SD from  $n = 2$  (other FC) or  $n = 4$  (red pulp and white pulp FC) biologically independent samples (depicted as symbols) examined over two independent experiments. Biological replicates represent cells sorted from pooled preparations from four mice. \*\*\* $p$ -value  $< 0.001$  (exact value indicated in the figure), two-tailed unpaired  $t$  test. q.l. quantification limit, n.d. not detected. Source data are provided as a Source Data file.

To this aim, we devised an ex vivo reactivation assay, in which PDGFR $\alpha^+$  FC isolated from the lungs of mice latently infected via intranasal route were seeded in half-area 96-well plates at the density of 100,000 cells per well (resulting in the deposition of ~100 MCMV genomes per well) (Fig. 4a). Upon 7 days of ex vivo incubation, viral reactivation was assessed in individual wells using three criteria: (i) visual inspection of plaque formation, (ii) IE1 immunofluorescence as well as (iii) detection of infectious virus in culture supernatant by plaque assay on monolayer of mouse embryonic fibroblasts (MEFs). Notably, infectious virus emerged in 30–50% of wells from 4 out of 4 samples of lung PDGFR $\alpha^+$  FC (Fig. 4b, c). As expected, virus did not grow out when lung PDGFR $\alpha^+$  FC isolated from mice infected intraperitoneally were used, as they were shown to be devoid of MCMV genomes (Fig. 4d, see also Fig. 1k). Further importantly, no virus outgrowth was detected when lysates prepared from lung PDGFR $\alpha^+$  FC isolated from mice infected intranasally were incubated on a monolayer of MEFs for the same amount of

time (Fig. 4e, f). The results showing that virus grew out only from cells but not from cell lysates (even though the assay was able to detect a single PFU of MCMV), argues that PDGFR $\alpha^+$  FC carried latent MCMV, which reactivated upon ex vivo cultivation. To confirm this using PDGFR $\alpha^+$  FC from another tissue, but also to study the kinetic of reactivation events, virus reactivation was also monitored in PDGFR $\alpha^+$  FC isolated from the VAT of mice latently infected via intraperitoneal route. Mice were administered with reporter MCMV expressing major IE promoter-driven GFP (MCMV<sup>IE-GFP</sup>)<sup>29</sup>, which resulted in the same latent viral load in VAT PDGFR $\alpha^+$  FC (Supplementary Fig. 4) while it enabled monitoring of the kinetic of re-initiation of lytic gene transcription by life cell imaging (Fig. 4g). By 7 days of in vitro incubation, the virus grew out in ~10% of wells from 9 out of 10 samples (Fig. 4h, i). Virus outgrowth was specifically associated with the presence of PDGFR $\alpha^+$  FC, since cultivation of VAT cell preparations that had been depleted of PDGFR $\alpha^+$  FC did not yield any virus (Fig. 4j). It should be

**Table 1 | Quantification of viral mRNAs in cell populations from latently infected mice by RT-qPCR**

Type of infection	Cell type	Estimated number of cells per reaction	MCMV transcript copies detected per reaction					
			<i>iel/3</i>	<i>M38</i>	<i>M48(SCP)</i>			
5 months after intraperitoneal infection	Spleen PDGFR $\alpha$ <sup>+</sup> FC	8911	n.d.	n.d.	n.d.	n.d.	n.d.	n.d.
		9153	n.d.	n.d.	n.d.	n.d.	n.d.	n.d.
		7630	n.d.	n.d.	n.d.	n.d.	n.d.	n.d.
	Visceral adipose tissue PDGFR $\alpha$ <sup>+</sup> FC	8359	n.d.	n.d.	n.d.	n.d.	n.d.	n.d.
		7659	21	8	n.d.	n.d.	n.d.	n.d.
		11,799	n.d.	n.d.	n.d.	n.d.	n.d.	n.d.
	Salivary gland PDGFR $\alpha$ <sup>+</sup> FC	5468	n.d.	n.d.	n.d.	n.d.	n.d.	n.d.
		6242	123	140	n.d.	n.d.	n.d.	n.d.
		6242	n.d.	n.d.	n.d.	9	58	60
	Liver PDGFR $\alpha$ <sup>+</sup> FC	6224	n.d.	n.d.	n.d.	n.d.	n.d.	n.d.
		6735	n.d.	n.d.	n.d.	n.d.	n.d.	n.d.
		6715	n.d.	n.d.	n.d.	n.d.	n.d.	n.d.
	Liver EC	9333	n.d.	n.d.	n.d.	n.d.	n.d.	n.d.
		6618	n.d.	n.d.	n.d.	n.d.	n.d.	n.d.
		9488	8	7	n.d.	n.d.	n.d.	n.d.
	Lung PDGFR $\alpha$ <sup>+</sup> FC (negative control)	14,431	n.d.	n.d.	n.d.	n.d.	n.d.	n.d.
		15,234	n.d.	n.d.	n.d.	n.d.	n.d.	n.d.
		16,971	n.d.	n.d.	n.d.	n.d.	n.d.	n.d.
5 months after intranasal infection	Lung PDGFR $\alpha$ <sup>+</sup> FC	16,971	200	128	n.d.	n.d.	n.d.	n.d.
		14,756	405	303	7	16	n.d.	n.d.
		17,261	317	433	n.d.	n.d.	n.d.	n.d.
3 months after intraperitoneal infection	Visceral adipose tissue PDGFR $\alpha$ <sup>+</sup> FC	10,626	10	14	n.d.	n.d.	n.d.	n.d.
		11,751	11	29	n.d.	n.d.	n.d.	n.d.
		9,498	40	64	n.d.	n.d.	n.d.	n.d.
	Visceral adipose tissue M $\phi$	10,551	n.d.	n.d.	n.d.	n.d.	n.d.	n.d.
		12,228	n.d.	n.d.	n.d.	n.d.	n.d.	n.d.
		10,975	5	5	n.d.	n.d.	n.d.	n.d.

Each row represents cDNA from a different biological replicate analysed in 2 reactions (technical duplicates) per MCMV gene. Biological replicates represent cells sorted from pooled preparations from 1 (lung, liver, salivary glands), 2 (visceral adipose tissue) or 4 (spleen) mice per replicate. n.d. not detected, MCMV murine cytomegalovirus, FC fibroblastic cells, M $\phi$  macrophages.

noted that this result does not provide evidence for the lack of reactivation from VAT M $\phi$  or EC since the culture conditions used were not optimized towards supporting survival of these cell types. As shown for lung PDGFR $\alpha$ <sup>+</sup> FC, virus was recovered only from live PDGFR $\alpha$ <sup>+</sup> FC from VAT and not from cell lysates (Fig. 4k, l). Thus, the virus could reactivate from PDGFR $\alpha$ <sup>+</sup> FC from both lungs and VAT, with frequency correlating with the level of IE gene transcription in these cells, which was lower in VAT than in the lungs (Table 1). Based on the emergence of initial GFP<sup>+</sup> cells, re-initiation of lytic gene transcription occurred either 1.5–2 days after seeding (50% of reactivations) or no sooner than 4–5 days after seeding (40% of reactivations) (Fig. 4m). Thus, reactivation events appeared to follow a biphasic kinetic. Together, these results indicate that MCMV latently persists in PDGFR $\alpha$ <sup>+</sup> FC in vivo.

### PDGFR $\alpha$ <sup>+</sup> FC are a site of lytic virus replication during primary MCMV infection

The apparent latent persistence of MCMV in PDGFR $\alpha$ <sup>+</sup> FC in vivo implied the question whether or not they could also support productive virus cycle during primary MCMV infection. To directly assess the permissiveness of PDGFR $\alpha$ <sup>+</sup> FC for lytic MCMV infection, we purified PDGFR $\alpha$ <sup>+</sup> FC from the lungs of naive mice and infected them ex vivo with recombinant MCMV<sup>AFP-CRBB</sup>, which expresses major IE promoter-driven green fluorescent protein (GFP) and late gene promoter-driven red fluorescent protein (mCherry) (Fig. 5a). Analysis of viral replication kinetics during in vitro culture demonstrated that PDGFR $\alpha$ <sup>+</sup> FC are permissive for lytic MCMV infection (Fig. 5b, c). To address this in vivo,

we first investigated if lytic gene expression was induced in PDGFR $\alpha$ <sup>+</sup> FC during the acute phase of infection with MCMV. Given that spleen becomes infected with MCMV within hours following intraperitoneal inoculation<sup>22</sup>, we isolated PDGFR $\alpha$ <sup>+</sup> FC from the spleens of mice 12 h post intraperitoneal infection, and analysed the expression of viral genes *iel/3*, *M38* and *M48(SCP)* by RT-qPCR. At 12 h post infection, splenic PDGFR $\alpha$ <sup>+</sup> FC expressed high levels of all three viral transcripts at levels at least 1000-fold higher than in any tested subset of PDGFR $\alpha$ <sup>+</sup> FC from latently infected mice (Table 2, see also Table 1). Therefore, splenic PDGFR $\alpha$ <sup>+</sup> FC supported lytic viral transcription shortly after the inoculation of mice with MCMV. To confirm that PDGFR $\alpha$ <sup>+</sup> FC also supported productive replication of the virus in vivo, we used mice heterozygous for *Pdgfra*-CreER<sup>T2</sup> knock-in allele<sup>40</sup> (hereafter termed *Pdgfra*-CreER<sup>T2</sup> (+/-)), that express tamoxifen-activatable Cre recombinase from one endogenous *Pdgfra* locus while the other locus is preserved, and infected them with a reporter virus MCMV<sup>flloxSTOP-GFP41</sup>. MCMV<sup>flloxSTOP-GFP</sup> undergoes deletion of the stop cassette preventing GFP expression in cells that express active Cre recombinase and was used previously with Tie2-Cre or Alb-Cre mice to define virus replication in endothelial cells or in hepatocytes<sup>41</sup>. Following the infection of *Pdgfra*-CreER<sup>T2</sup> (+/-) mice with MCMV<sup>flloxSTOP-GFP</sup> it is expected that the viruses that replicate in PDGFR $\alpha$ <sup>+</sup> FC become genetically recombined so their progeny gives rise to GFP<sup>+</sup> plaques on monolayers of MEFs. *Pdgfra*-CreER<sup>T2</sup> (+/-) mice were infected with MCMV<sup>flloxSTOP-GFP</sup> via the intraperitoneal route on day 0, fed tamoxifen from -1 to 3 days post infection to activate the Cre recombinase, and sacrificed on day 4 post

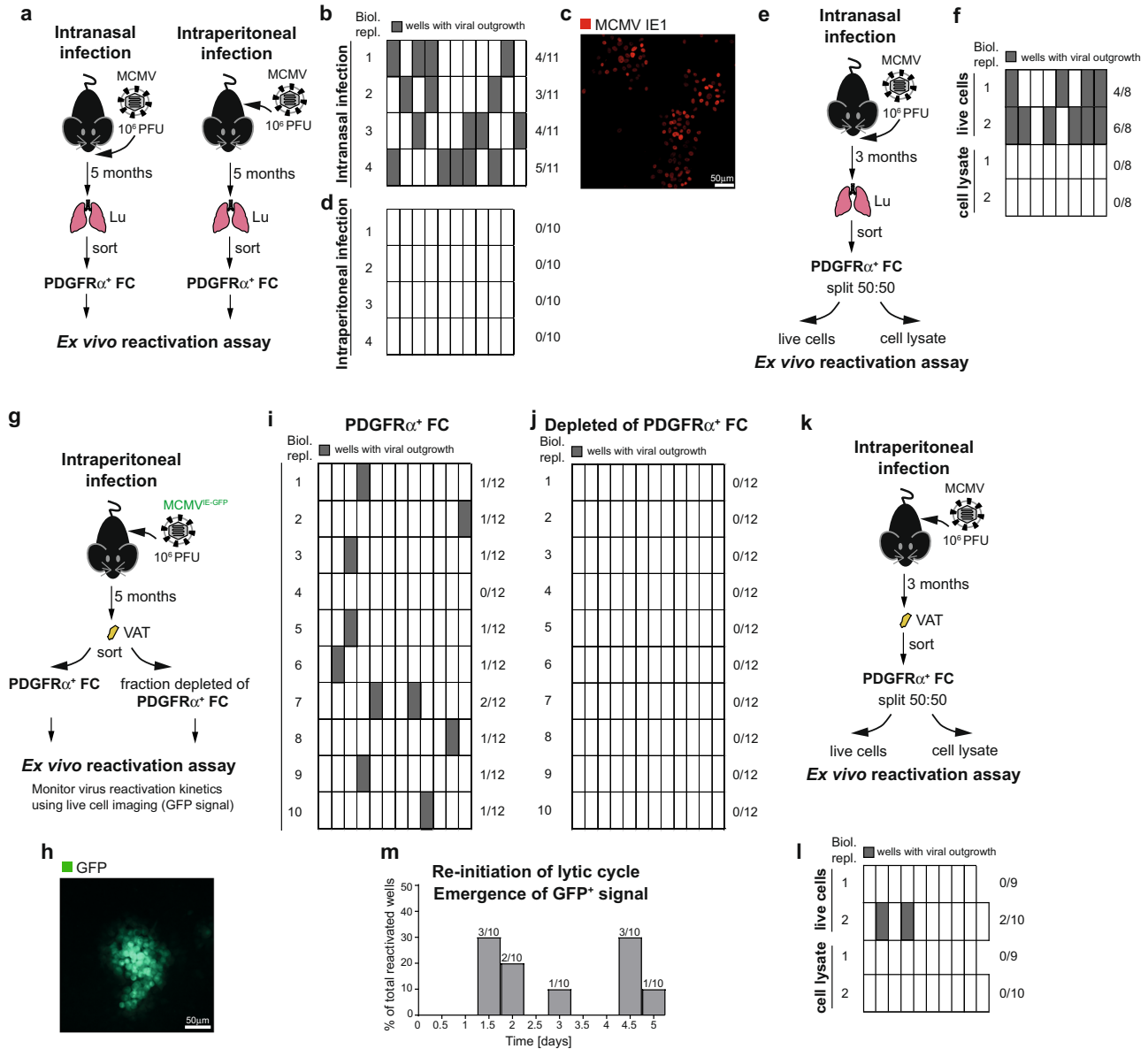


**Fig. 4 | MCMV establishes latent infection in PDGFR $\alpha^+$  FC in vivo.** Ex vivo virus reactivation assay from PDGFR $\alpha^+$  FC purified from (a–f), the lungs of mice latently infected with MCMV administered intranasally or (g–m), from the VAT of mice latently infected with MCMV administered intraperitoneally. **a** Experimental design for (b–d). **e** Experimental design for (f). **g** Experimental design for (h–j, m). **k** Experimental design for (l). **b, d, f, i, j, l** Frequency of viral outgrowth from wells with indicated cells. Biologically independent replicates are from 1 to 2 mice per

replicate. Numbers on the right side are the proportion of wells with virus outgrowth for the indicated biological replicate. **c** Representative immunofluorescence image showing detection of viral IE1 protein. **h** Representative fluorescence microscopy image of a GFP $^+$  plaque that arose in the ex vivo reactivation assay. **m** Kinetic of re-initiation of viral lytic cycle. Shown is the proportion of wells in which GFP signal had first emerged at the indicated time-point.

infection (Fig. 5d). Organ lysates from the spleen, VAT, liver and lungs were used to determine the frequency of GFP $^+$  plaques. On day 4 post infection, GFP $^+$  virus was detected as ~10% of plaques in the liver, ~20% in the VAT and ~50% in the spleen and lungs, although in the latter organ the percentage of GFP $^+$  plaques could only be reliably measured in 5 out of 10 samples due to generally low infectious virus titer in this organ (Fig. 5e, f). The emergence of GFP $^+$  virus was entirely dependent on the presence of Cre recombinase since similar virus titer but no GFP $^+$  plaques were found in organs of infected Cre-negative littermate controls (Supplementary Fig. 5a–b). Thus, multiple organs contained the progeny of viruses that had replicated in PDGFR $\alpha^+$  cells, indicating that PDGFR $\alpha^+$  FC play a role in MCMV in vivo replication. Of note, given that MCMV may have spread from the sites of initial replication within 4 days, it is not possible to distinguish whether the virus had replicated

in PDGFR $\alpha^+$  FC present in the given organ or elsewhere. In sum, PDGFR $\alpha^+$  FC supported both productive infection and latent MCMV persistence in vivo.

### Stat1 is required for MCMV genome persistence in fibroblastic cells in vivo

Next, we sought to identify host pathway/s that affect MCMV's ability to latently persist in PDGFR $\alpha^+$  FC in vivo. We hypothesized that the same signal/s that inhibit lytic cycle entry by MCMV may concomitantly enable the virus to establish and/or maintain latent infection. Since IFN $\beta$  is sufficient to silence IE transcription<sup>20</sup>, we chose to assess the putative involvement of STAT1, which crucially mediates responses to IFNs<sup>16</sup> by testing lytic and latent MCMV infection in *Stat1* $^{-/-}$  mice. To circumvent the caveats linked to the increased sensitivity of



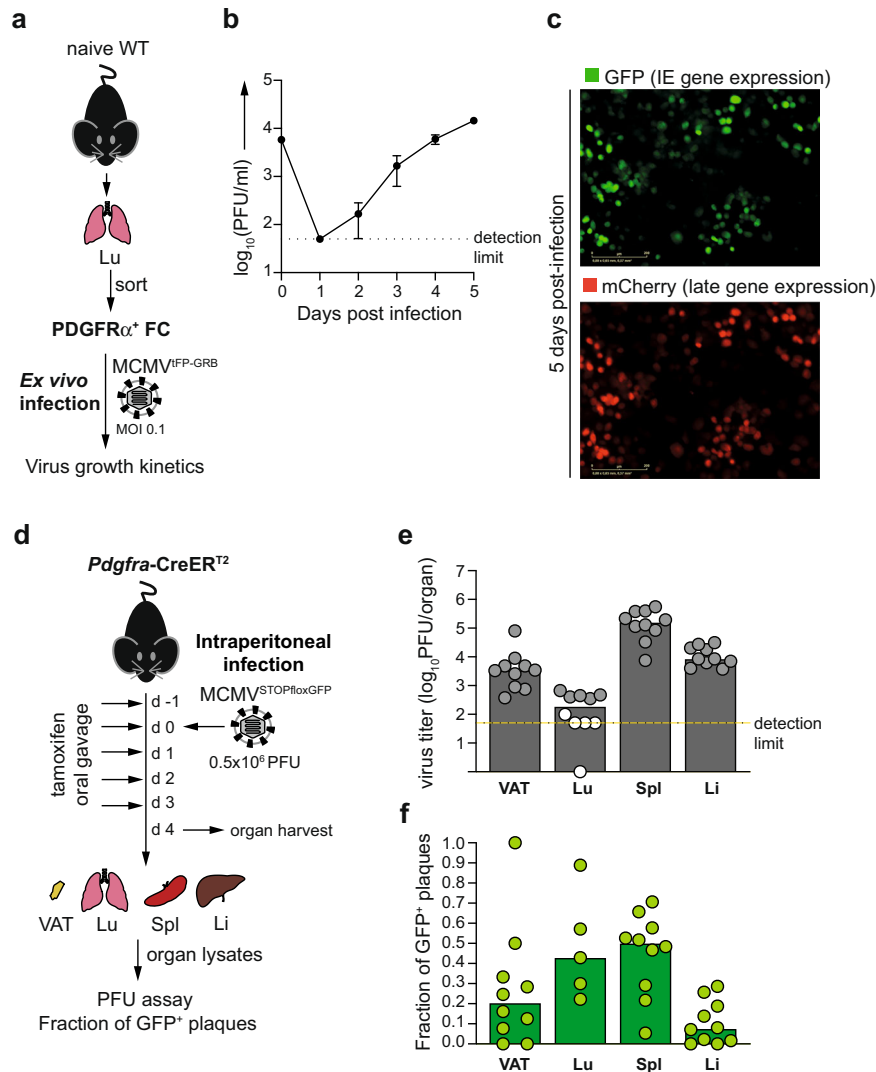


**Fig. 5 | PDGFR $\alpha$  FC are a site of lytic virus replication during primary MCMV infection.** **a–c** Analysis of virus replication kinetics in lung-derived PDGFR $\alpha$  FC following their ex vivo infection with MCMV<sup>IEFP-GRB</sup>, which expresses IE promoter driven-green fluorescent protein (GFP) and late gene promoter-driven red fluorescent protein (mCherry). **a** Experimental design for **(b, c)**. **b** Data are presented as arithmetic mean  $\pm$  SD of  $n = 3$  technical replicates and are from one representative experiment of 2 using cells sorted from pooled lung preparations from 3 mice. **c** Representative fluorescence microscopy images of GFP and mCherry expression 5 days after ex vivo infection. **d–f** Contribution of PDGFR $\alpha$  FC to MCMV

propagation in vivo determined after intraperitoneal infection of *Pdgfra*-CreER<sup>T2</sup> (+/-) mice with a Cre-inducible reporter virus, MCMV<sup>flaxSTOP-GFP</sup>. **d** Experimental design for **(e, f)**. **e** Median virus titer in indicated organs. Circles represent samples from individual mice. Grey-filled circles are samples with sufficient virus titer to enable examination of GFP<sup>+</sup> plaques. White-filled circles are samples in which virus titer was too low to enable examination of GFP<sup>+</sup> plaques. **f** Median proportion of GFP<sup>+</sup> plaques in indicated organs. Circles represent samples from individual mice. Source data are provided as a Source Data file.

**Table 2 | Quantification of viral mRNAs in cell populations from acutely infected mice by RT-qPCR**

Type of infection	Cell type	Estimated number of cells per reaction	MCMV transcript copies detected per reaction					
			<i>ie1/3</i>		<i>M38</i>		<i>M48(SCP)</i>	
12 h after intraperitoneal infection	Spleen PDGFR $\alpha$ FC	7944	219,224	211,938	411,485	411,485	61,694	61,289
Uninfected	Spleen PDGFR $\alpha$ FC	6113	n.d.	n.d.	n.d.	n.d.	n.d.	n.d.

cDNA isolated from pooled cell preparations from 4 mice was analysed in 2 technical duplicates per MCMV gene. n.d. not detected, MCMV murine cytomegalovirus, FC fibroblastic cells.

*Stat1*<sup>-/-</sup> mice to MCMV, we generated and used a single-cycle GFP-reporter MCMV mutant, which we name MCMV<sup>AgL-GFP</sup>. To this effect we disrupted the gene for the essential virion glycoprotein L (gL/M15) in our GFP reporter virus, MCMV<sup>IEI/3-GFP29</sup> on a  $\Delta$ m157 background. MCMVs lacking gL can be propagated in gL-complementing cells, to generate virus stocks consisting of pseudotyped gL<sup>+</sup> virions that are able to

infect and replicate for one cycle in gL deficient cells, whereupon their progeny virions will lack the gL and thus cannot spread further to other cells<sup>42–44</sup>. As shown in Fig. 6a, WT and *Stat1*<sup>-/-</sup> mice were infected with MCMV<sup>AgL-GFP</sup>, followed by analysis of lytic infection and latent persistence of the virus respectively at 22 h and 60 days post infection in fibroblastic cells in the spleen, which are known to be directly infected

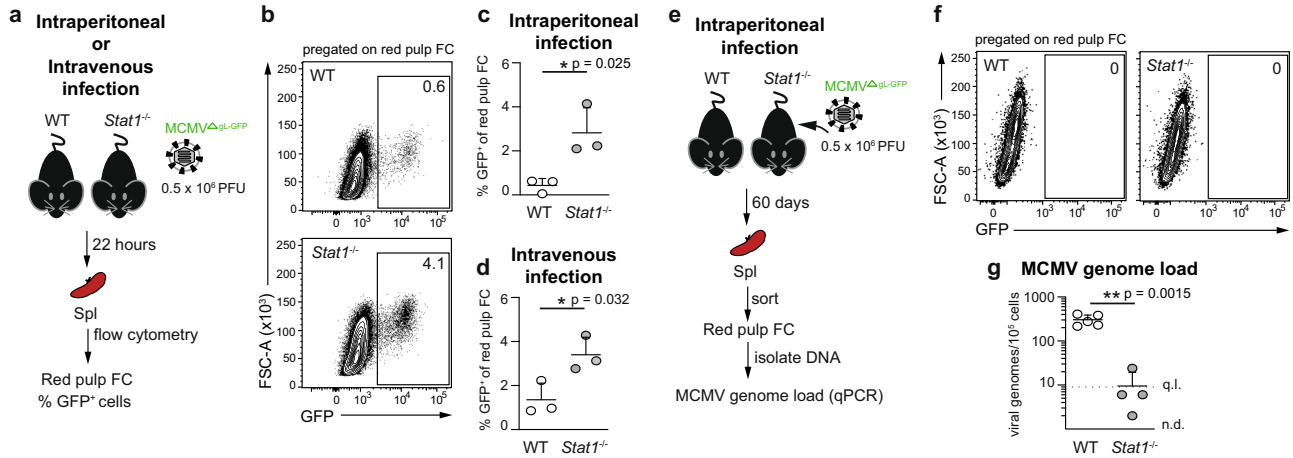


**Fig. 6 | *Stat1* is required for MCMV genome persistence in fibroblastic cells in vivo.** **a–d** Analysis of the lytic infection of red pulp FC in WT and *Stat1*<sup>-/-</sup> mice 22 h after the administration of MCMV<sup>ΔgI-GFP</sup> intraperitoneally or intravenously. **a** Experimental design for **(b–d)**. **b–d** Percentage of GFP<sup>+</sup> cells in red pulp FC. **b** Representative flow cytometry plot. Numbers indicate the percentage of gated cells. **c, d** Data are presented as the arithmetic mean ± SD of *n* = 3 biologically independent mice (depicted as symbols) examined over one experiment performed for each infection route. \**p*-value < 0.05 (exact *p* value indicated in the plot), two-tailed unpaired *t* test. **e–g** Analysis of latent MCMV persistence in red

pulp FC from WT and *Stat1*<sup>-/-</sup> mice 60 days after intraperitoneal administration of MCMV<sup>ΔgI-GFP</sup>. **e** Experimental design for **(f, g)**. **f** Plots show the lack of GFP<sup>+</sup> cells in red pulp FC. **g** Number of virus genomes per 100,000 of red pulp FC. Horizontal line depicts arithmetic mean ± SD from *n* = 4 biologically independent samples (depicted as symbols) examined over two independent experiments. Biological replicates represent cells sorted from pooled preparations from two mice. \*\**p*-value < 0.01 (exact *p* value indicated in the plot), two-tailed Welch's *t* test. q.l. quantification limit, n.d. not detected. Source data are provided as a Source Data file.

**Table 3 | Quantification of viral mRNAs in cell populations from WT and *Stat1*<sup>-/-</sup> mice by RT-qPCR**

Type of infection	Cell type	Estimated number of cells per reaction	MCMV transcript copies detected per reaction					
			<i>ie1/3</i>	<i>M38</i>	<i>M48(SCP)</i>			
22 h after intravenous infection with MCMV <sup>ΔgI-GFP</sup>	GFP <sup>+</sup> WT red pulp FC	310	72,214	73,673	677,316	713,744	65,231	60,544
		470	151,387	139,745	1,253,481	1,278,349	100,668	114,507
		201	35,075	31,316	369,285	355,057	42,951	42,372
	GFP <sup>+</sup> <i>Stat1</i> <sup>-/-</sup> red pulp FC	242	82,357	79,127	1,208,111	1,281,450	102,291	98,214
		311	41,163	36,264	710,806	724,908	44,131	44,734
		518	59,401	65,214	905,681	999,157	66,734	65,391
60 days after intraperitoneal infection with MCMV <sup>ΔgI-GFP</sup>	WT red pulp FC	21,864	n.d.	n.d.	n.d.	4	n.d.	n.d.
		18,811	n.d.	n.d.	n.d.	n.d.	n.d.	n.d.
		17,837	n.d.	n.d.	n.d.	n.d.	n.d.	n.d.
		16,063	n.d.	n.d.	n.d.	n.d.	n.d.	n.d.
		18,503	n.d.	n.d.	n.d.	n.d.	15	n.d.
	<i>Stat1</i> <sup>-/-</sup> red pulp FC	23,573	n.d.	n.d.	n.d.	n.d.	n.d.	n.d.
		21,565	n.d.	n.d.	n.d.	n.d.	n.d.	n.d.
		17,029	n.d.	n.d.	n.d.	n.d.	n.d.	n.d.
		25,591	n.d.	n.d.	n.d.	n.d.	n.d.	n.d.
			n.d.	n.d.	n.d.	n.d.	n.d.	n.d.

Each row represents cDNA from a different biological replicate analysed in 2 reactions (technical duplicates) per MCMV gene. Biological replicates represent cells sorted from a single mouse in single experiment (22 hours post infection) or cells sorted from pooled preparations of 2 mice and are from 2 independent experiments (60 days post infection). n.d. not detected, MCMV murine cytomegalovirus, FC fibroblastic cells.

by MCMV virions injected intraperitoneally or intravenously<sup>22</sup>. We focused specifically on red pulp FC, firstly because their high MCMV genome content during in vivo latency offered a broad dynamic range and secondly, to eliminate confounding effects due to a potential change in the composition of spleen stromal cells in *Stat1*<sup>-/-</sup> mice. Since Ly6C is an IFN-regulated gene, Ly6C<sup>+</sup> red pulp FC were identified as PDGFRα<sup>+</sup>BST-1<sup>+</sup>CD146<sup>-</sup> FC, as previously reported<sup>29</sup>. The abundance of red pulp FC was comparable between WT and *Stat1*<sup>-/-</sup> mice (Supplementary Fig. 6a). At 22 hours after intraperitoneal injection of MCMV<sup>ΔgI-GFP</sup>, *Stat1*<sup>-/-</sup> mice showed a higher percentage of GFP<sup>+</sup> red pulp FC (unpaired *t*-test, degrees of freedom = 4, *p* = 0.025, 95% CI of the difference = 0.4917–4.295) (Fig. 6b, c). This phenotype was not a result

of putative differences in the transport of the virus from the peritoneum to the spleen between WT and *Stat1*<sup>-/-</sup> mice since the percentage of GFP<sup>+</sup> red pulp FC was also elevated in *Stat1*<sup>-/-</sup> mice following intravenous injection of MCMV<sup>ΔgI-GFP</sup> (unpaired *t*-test, degrees of freedom = 4, *p* = 0.0324, 95% CI of the difference = 0.2798–3.807) (Fig. 6d). Consistent with being lytically infected, GFP<sup>+</sup> red pulp FC sorted from WT and *Stat1*<sup>-/-</sup> mice 22 h post infection expressed high levels of *ie1/ie3*, *M38* and *M48(SCP)* transcripts (Table 3). Therefore, more red pulp FC became lytically infected in the absence of STAT1. At 60 days post infection (Fig. 6e), red pulp FC were devoid of GFP<sup>+</sup> cells (Fig. 6f) and viral gene expression was silenced (Table 3). Notably, whereas MCMV genomes persisted in red pulp FC from WT mice, red pulp FC were

depleted of MCMV genomes in *Stat1*<sup>-/-</sup> mice (unpaired *t*-test with Welch's correction, degrees of freedom = 4.126, *p* = 0.0015, 95% CI of the difference = -402.4 to -185.8) (Fig. 6g). This difference was not present at the onset as indicated by the undiminished viral genomic loads in both GFP<sup>+</sup> and GFP<sup>-</sup> red pulp FC from *Stat1*<sup>-/-</sup> mice at 22 h post infection (Supplementary Fig. 6b). Together, the above data implicate a dual role of STAT1 as a negative regulator of lytic MCMV infection and a positive regulator of latent MCMV persistence in fibroblastic cells *in vivo*. Whether the *Stat1*-dependency of latent MCMV persistence in fibroblastic cells *in vivo* results from putative direct regulation of MCMV latency by STAT1 or whether it is due to other putative cell intrinsic or extrinsic effects of STAT1, such as regulation of infected cell survival or their immune control, will require clarification by future studies.

## Discussion

This work provides a comprehensive characterisation of the distribution of MCMV genomes in multiple tissue-resident cell types across numerous organs during MCMV latency *in vivo*, and the demonstration of latent MCMV persistence in fibroblastic cells. Latent MCMV persistence in PDGFR $\alpha$ <sup>+</sup> FC was not restricted to a single organ but represented a wide-spread phenomenon engaging many organs, suggesting that fibroblasts are a physiologically relevant, and in some organs may be a major site of MCMV latency. Our findings are not in opposition with previous identification of endothelial cells and macrophages as cellular sites of MCMV latency *in vivo* but rather confirm and extend previous knowledge by broadening the scope of tissues in which these cell types were tested for MCMV genome presence. In our model, which involved infection of adult C57BL/6 mice with tissue culture-derived MCMV, we found the content of MCMV genomes in monocytes to be below 10 copies per 100,000 cells at 5 months post infection. This is similar to a recent study by Liu et al., in which 3-week-old BalbC mice were infected with MCMV Smith strain and analysed 3-6 months later, where the MCMV genome load in monocytes was more robust but still not higher than 10 copies per 100,000 cells<sup>7</sup>. It has been suggested that the presence of latent HCMV in endothelial cells may be a consequence of transdifferentiating latently infected myeloid progenitor cells<sup>45</sup>, which might in theory explain our observations. However, the scarcity of viral genomes in monocytes in relation to tissue-resident cells, argues against this explanation in MCMV latency. Furthermore, given modern knowledge about the origin of fibroblastic cells in the mouse we deem this scenario very unlikely for MCMV. It is currently well established that CD45<sup>+</sup>PDGFR $\alpha$ <sup>+</sup> or PDGFR $\beta$ <sup>+</sup> fibroblastic cells found in mouse organs under homeostatic conditions are mesenchymal-derived and not a progeny of circulating progenitors originating from hematopoietic or mesenchymal BM-derived stem cells<sup>27</sup>. Although differentiation of monocyte/M $\phi$ -like cells into fibroblasts has been documented in the context of organ injury or fibrosis<sup>46,47</sup>, the low MCMV content of monocytes and M $\phi$  in most studied organs is at odds with the high enrichment of CD45<sup>+</sup>PDGFR $\alpha$ <sup>+</sup> for MCMV genomes observed in our study. An alternative hematopoietic source of fibroblast-like cells in a perturbed state can be CD34<sup>+</sup>Col1a1<sup>+</sup> fibrocytes, but they and their progeny were excluded from our analysis based on their positivity for CD45<sup>48</sup>. Thus, available indirect evidence strongly suggests that MCMV not only latently persist in but also latently infects CD45<sup>+</sup>PDGFR $\alpha$ <sup>+</sup> FC.

Notably, PDGFR $\alpha$ <sup>+</sup> FC also became lytically infected by the virus and contributed to its *in vivo* replication during the acute stage following primary infection. These findings shed light on the role of fibroblasts in MCMV's life cycle *in vivo* by showing that not only does this cell type support viral lytic cycle, as previously understood, but it nevertheless serves as the site of latent MCMV persistence. It is important to note that the above conclusion can only be inferred for the entire population of PDGFR $\alpha$ <sup>+</sup> FC from a given organ, but not on a single-cell basis. PDGFR $\alpha$ <sup>+</sup> FC are known to be heterogenous<sup>32</sup> and it is

entirely possible that lytic and latent infection are allocated to distinct subsets or maturation stages. Additional studies involving single-cell transcriptomics will be required to resolve this matter in the future.

While our study was focused on demonstrating bone-fide latent virus persistence in fibroblastic cells and identification of a cellular signalling pathway on which it is critically dependent, several important follow-up questions remain that lie outside of the scope of the current project. For instance, although our studies in *Stat1*<sup>-/-</sup> mice unravel that STAT1 is required to enable latent persistence of MCMV in fibroblastic cells *in vivo*, we did not determine whether or not this requirement is cell intrinsic. To decipher this, mice bearing conditional deletion of *Stat1* in fibroblasts will need to be implemented. Should STAT1 be specifically required in fibroblasts, it will further need to be clarified whether it directly regulates viral latent persistence. Addressing these questions will require careful probing of single-cell transcriptomes of fibroblastic cells at various time points after infection *in vitro* or *in vivo*. Regardless of the results of future investigations addressing these outstanding questions, it is important to observe that the data generated in the course of this study unravel that one of the most prominent antiviral host factors, which is crucial for the resolution of virus infections and host survival, concomitantly enables a herpesvirus to latently persist in its host, at least in certain cell types. In sum, the findings of this study significantly broaden our understanding of the functions of murine STAT1 during *in vivo* infection with a  $\beta$ -herpesvirus.

## Methods

### Mice

C57BL/6JrJ mice were purchased from Janvier Labs. B6.129S-*Pdgfra*<sup>tm1.1(Cre/ERT2)BIR/J</sup> mice<sup>40</sup> on C57BL/6J background were purchased from the Jackson Laboratory (IMSR\_JAX:032770) and used in comparison to littermate controls. *Stat1*<sup>-/-</sup> mice on C57BL/6N background<sup>49</sup> and C57BL/6N controls were kindly provided by Birgit Strobl and Mathias Müller, University of Veterinary Medicine Vienna, Vienna, Austria. Mice were bred and maintained under specific pathogen free (SPF) conditions according to Federation of European Laboratory Animal Science Associations (FELASA) guidelines at central animal facility of HZI Braunschweig, Germany; Faculty of Medicine, University of Rijeka, Croatia, and University of Veterinary Medicine Vienna, Austria. Animal procedures were approved as due by The Lower Saxony State Office of Consumer Protection and Food Safety; by The Ethics Committee at the Faculty of Medicine, Rijeka and Ethics Committee of the Veterinary Department of the Ministry of Agriculture, Croatia, and by the Ethics and Animal Welfare Committee of the University of Veterinary Medicine Vienna and the Austrian Federal Ministry of Science and Research. Mice were maintained on a 12-h light and dark cycle at 21 °C and 55% humidity. The study used female mice due to the cytotoxicity of salivary gland homogenates from male mice, which impairs virus titrations from this organ. Mice were infected at 8–10 weeks of age, except in Fig. 6 where the infection was done at 14 weeks of age. Virus was administered in 200  $\mu$ l PBS intraperitoneally or in 20  $\mu$ l in PBS intranasally<sup>36</sup>. *Pdgfra*-CreER<sup>12</sup> mice received tamoxifen (0.1 mg/g; Sigma) diluted in corn oil by oral gavage daily from day -1 to day 3 post-infection.

### Viruses

Viral stocks were generated in tissue culture by transfecting MCMV genome-carrying BACs into NIH3T3 cells (ATCC CRL-1658) using FuGene HD (Promega). Reconstituted viral particles were passaged five times on M2-10B4 cells (ATCC CRL-1972) before generating sucrose cushion-purified viral stocks. All MCMVs used in this study were based on the Mck2-repaired BAC-encoded MCMV strain, clone pSM3fr-MCK-2fl 3.3<sup>50</sup>. MCMV<sup>IE-GFP29</sup> and MCMV<sup>flloxSTOP-GFP41</sup> were described before. MCMV<sup>GFP-GRB</sup> expressing three different fluorescent proteins under the control of endogenous viral promoters was generated by *en passant*

mutagenesis<sup>51</sup> using expression cassettes described earlier<sup>52</sup>. In short, constructs encoding fluorescent reporters (EGFP, mTagBFP-NLS and mCherry) plus a distal P2A-encoding sequence were inserted into the start codon of IE1/3 (EGFP), E2 (mTagBFP-NLS), and SCP (mCherry). MCMV<sup>AgL.GFP</sup> was generated by disrupting m157 and gL/M115 genes in MCMV<sup>IE-GFP</sup>. Viral genes were disrupted by frameshift mutations induced by replacement of 38 bp of each gene's open reading frame (ORF) with two STOP codons targeted to the ORF's start (gL) or after codon 22 (m157). MCMV<sup>AgL.GFP</sup> was propagated in gL-expressing NIH-3T3 cell line<sup>42</sup> (a kind gift from Ian Humphreys, Cardiff University).

### Cell isolation

Peri-gonadal VAT was digested with collagenase P (0.4 mg/ml), dispase II (2 mg/ml) and DNase I (50 µg/ml) in high-glucose GlutaMAX-supplemented DMEM with 10 mM HEPES and 4% fatty acid-free BSA (Sigma-Aldrich) for 55 min at 37 °C. The suspension was passed through a 100 µm nylon mesh filter (BD Biosciences), and the floating adipocyte fraction was removed by centrifugation at 400 × g for 6 min. Spleen, LNs and SGs were processed according to a previously established protocol<sup>29</sup>. In short, enzymatic treatment with collagenase P (0.4 mg/ml), dispase II (2 mg/ml) and DNase I (50 µg/ml) was performed for 30 min at 37 °C and then repeated for an additional 20 min, followed by incubation with 5 mM EDTA for 5 min. CD45<sup>+</sup> cell fractions from the spleen and LNs were enriched by depletion of CD45<sup>+</sup> cells while splenic Mφ were enriched by positive selection of VCAM-1<sup>+</sup> cells using MACS (Miltenyi Biotech). Lungs were injected with 2.5 ml digestion solution containing collagenase P (0.4 mg/ml), dispase II (2 mg/ml) and DNase I (50 µg/ml), minced with scissors and then processed in gentleMACS Dissociator (Miltenyi Biotech) using program "37C\_m\_LDK\_1". Liver digestion was performed using the retrograde perfusion technique via the inferior vena cava described by Mederacke et al.<sup>30</sup> with modifications. Briefly, organs were in situ perfused with 10 ml of pre-warmed Liver Perfusion Medium (Gibco) followed by injection of 20 ml of pre-warmed digestion medium (1 mg/ml collagenase P, 1 mg/ml dispase II, 50 µg/ml DNase I in Gibco Hank's Balanced Salt Solution (HBSS) with 10 mM HEPES and 1.5 mM calcium chloride) over 5–7 min. Afterwards, organs were dissected, minced with scissors and in vitro digested for 45 min at 37 °C. Non-parenchymal cells were enriched by two rounds of centrifugation at 50 × g for 5 min whereupon only supernatant was collected.

### Flow cytometry and cell sorting

Antibodies used in this study are listed in Supplementary Table 2. Dead cells (identified using 7-AAD or Zombie Fixable Viability Kits; both from BioLegend) and cell aggregates (identified on FSC-A versus FSC-H scatter plots) were excluded from all analyses. Sorting was performed on ARIA-Fusion, Aria-II SORP or Aria-II (BD Biosciences). Analysis was done using FlowJo software (version 10, BD Biosciences).

### Immunofluorescence

Cells were fixed in 4% (wt/vol) paraformaldehyde, permeabilized in 0.1% Triton-X and blocked with 2% BSA. Staining with anti-IE1 antibody (IE 1.O1, CapRi) was done overnight at 4 °C and was followed by incubation with anti-mouse IgG (H + L) F(ab')<sub>2</sub> conjugated to Alexa Fluor 647 (Cell Signaling Technology). Images were acquired with ZEISS LSM 980 laser-scanning confocal microscope and analysed using ZEN blue (ZEN lite) version 3.5.093.0004 (Carl Zeiss MicroImaging).

### Quantification of MCMV genome load by qPCR

Quantification of MCMV genome load was performed according to the method described by Simon et al.<sup>33</sup> with modifications. Briefly, DNA was extracted using AllPrep DNA/RNA Micro Kit (QIAGEN), and after elution precipitated with ethanol, washed, and resuspended in 40 µl dH<sub>2</sub>O. Samples were assayed for viral gB and mouse Pthrp DNA copies in technical duplicates using 9 µl of sample DNA per reaction. Serial

dilutions of 10<sup>6</sup>–10<sup>1</sup> copies per reaction of the pDrive\_gB\_PTHrP\_Tdy plasmid<sup>33</sup> were used to generate standard curves for both qPCR reactions. Dilutions of 10<sup>4</sup>–10<sup>1</sup> plasmid copies contained 1 ng carrier RNA (QIAGEN). QPCR was performed in a LightCycler 480 Instrument II (software version 1.5.0.39, Roche) using Fast Plus EvaGreen qPCR master mix (Biotium). Cycling conditions were as follows: enzyme activation, 2 min 95 °C, followed by 50 cycles of denaturation for 10 s at 95 °C, annealing for 20 s at 56 °C and extension for 30 s at 72 °C. Specificity of amplified sequences was validated by inspection of melting curves. Primer sequences: *Pthrp* 5'-ggatctgccctcatgctgctg-3' and 5'-cgtttctctccaccatctg-3'; gB 5'-gcagctagctgctttctgc-3' and 5'-aggcgtggactagcgataa-3'.

### Analysis of MCMV transcripts by RT-qPCR

Total RNA was extracted using AllPrep DNA/RNA Micro Kit with on-column DNA removal (QIAGEN). cDNA was synthesized with SuperScript IV Reverse Transcriptase and a 1:1 mixture of oligo-dT and random oligonucleotide hexamers (Invitrogen). QPCR was performed in a LightCycler 480 Instrument II (software version 1.5.0.39, Roche) using Fast Plus EvaGreen qPCR master mix (Biotium). Serial dilutions of 10<sup>6</sup>–10<sup>1</sup> copies per reaction of MCMV genome containing BAC (clone pSM3fr-MCK-2fl 3.3<sup>50</sup>) were used to generate standard curves. Dilutions of 10<sup>1</sup>–10<sup>4</sup> BAC copies contained 1 ng carrier RNA (QIAGEN). Cycling conditions were as follows: enzyme activation, 2 min 95 °C, followed by 50 cycles of denaturation for 10 s at 95 °C, annealing for 20 s at 57 °C and extension for 30 s at 72 °C. Specificity of amplified sequences was validated by inspection of melting curves. RT-qPCR reactions prepared from equal amount of sample RNA but with the omission of reverse transcriptase served as controls for the absence of carry-over viral DNA. Primer sequences: *Gapdh* 5'-tgtgtccgtcgtggatctga-3' and 5'-cctgcttaccaccttctgat-3'; *ie1/3* 5'-ggcgtgaagtgtgggtaca-3' and 5'-cgcatcgaagac aacgcaa-3'; *M38* 5'-cccattgccacgttttgggtg-3' and 5'-tctcaagtgcacatcgctca-3'; *M48/SCP* 5'-aggacgtgttgaaacttctctcc-3' and 5'-tcgatgtccgtctctctcac-3'.

### Ex vivo reactivation assay

FC were seeded into fibronectin-coated 96 Half Area Well Flat Bottom Microplates (Corning) (lung FC) or gelatin- or fibronectin-coated 96 Well Flat Bottom Microplates (Greiner Bio-One) (VAT FC) at a density of 100,000 cells per well in culture medium (high-glucose DMEM supplemented with 1% (vol/vol) GlutaMAX, 10 mM HEPES, 50 µM 2-mercaptoethanol, 200 U/ml penicillin, 200 U/ml streptomycin, 50 µg/ml gentamicin and 5% FCS) and incubated in a humidified incubator under 5% CO<sub>2</sub> and at 37 °C for 7 days without replacing the medium. Cell lysates prepared in gentleMACS M Tubes for tissue homogenisation using gentleMACS Dissociator (Miltenyi Biotech, program "mlung\_02") were assayed in parallel by incubation with MEFs. To track the emergence of GFP<sup>+</sup> cells, plates were imaged with InCuCyte S3 v2021B automated fluorescence microscope (Sartorius). After 7 days, plates were directly inspected for the presence of plaques and additionally, the culture supernatant from each well was tested for the presence of infectious virus by plaque assay on MEFs. To ensure detection of even minimal amounts of virus<sup>53</sup>, following the addition of the supernatant, MEFs were spun down at 800 × g for 30 min and then incubated at 37 °C for another 30 min. Afterwards, the inoculum was removed and the cells overlaid with medium containing 0.75% (wt/vol) methylcellulose (Sigma). After 4 days at 37 °C, the plates were examined for the presence of plaques under an inverted microscope.

### Ex vivo infection of cells

Lung-derived FC at 80% confluency were infected with MCMV<sup>IEP-GRB</sup> at an MOI of 0.1 for an hour at 37 °C. Afterwards, the medium was changed to cultivation medium (high-glucose DMEM (Gibco) supplemented with 1% (vol/vol) GlutaMAX, 10 mM HEPES, 50 µM 2-mercaptoethanol, 200 U/ml penicillin, 200 U/ml streptomycin, 50 µg/ml gentamicin and 5% FCS). Supernatants were collected from



a different set of wells every 24 h until 5 days post infection and stored at  $-80^{\circ}\text{C}$ . In addition, plates were imaged with IncuCyte S3 v2021B automated fluorescence microscope (Sartorius). Titration of the virus was done by infecting MEF cell monolayers grown in 48-well plates with serially diluted supernatants for an hour at  $37^{\circ}\text{C}$ . Thereupon, the inoculum was removed, and the cells were overlaid with a culture medium containing 0.75% (wt/vol) methylcellulose (Sigma). Plaques were counted following incubation of cells for 4 days at  $37^{\circ}\text{C}$ .

### Statistics and reproducibility

Statistical analysis was performed with GraphPad Prism 9. Results were reproduced by at least two independent experiments and all repeats were successful. No data were excluded from the analyses. No statistical method was used to predetermine the sample size. Mice were allocated to groups based on genotype. The investigators were not blinded to allocation during experiments as this was not deemed necessary since the type of readouts were not subjective and also to avoid/control for cross-contamination of the samples.

### Reporting summary

Further information on research design is available in the Nature Portfolio Reporting Summary linked to this article.

### Data availability

All other relevant data supporting the key findings of this study are available within the article and its Supplementary Information files. Source data are provided with this paper.

### References

- Gatherer, D. et al. ICTV Virus Taxonomy Profile: Herpesviridae 2021. *J. Gen. Virol.* **102**, 001673 (2021).
- Liu, X. F., Yan, S., Abecassis, M. & Hummel, M. Establishment of murine cytomegalovirus latency in vivo is associated with changes in histone modifications and recruitment of transcriptional repressors to the major immediate-early promoter. *J. Virol.* **82**, 10922–10931 (2008).
- Sinclair, J. Chromatin structure regulates human cytomegalovirus gene expression during latency, reactivation and lytic infection. *Biochim. Biophys. Acta* **1799**, 286–295 (2010).
- Reddehase, M. J., Podlech, J. & Grzimek, N. K. Mouse models of cytomegalovirus latency: overview. *J. Clin. Virol.* **25**, S23–S36 (2002).
- Cohen, J. I. Herpesvirus latency. *J. Clin. Invest.* **130**, 3361–3369 (2020).
- Griffiths, P. & Reeves, M. Pathogenesis of human cytomegalovirus in the immunocompromised host. *Nat. Rev. Microbiol.* **19**, 759–773 (2021).
- Liu, X. F. et al. A novel murine model of differentiation-mediated cytomegalovirus reactivation from latently infected bone marrow haematopoietic cells. *J. Gen. Virol.* **100**, 1680–1694 (2019).
- Seckert, C. K. et al. Liver sinusoidal endothelial cells are a site of murine cytomegalovirus latency and reactivation. *J. Virol.* **83**, 8869–8884 (2009).
- Brautigam, A. R., Dutko, F. J., Olding, L. B. & Oldstone, M. B. Pathogenesis of murine cytomegalovirus infection: the macrophage as a permissive cell for cytomegalovirus infection, replication and latency. *J. Gen. Virol.* **44**, 349–359 (1979).
- Pollock, J. L., Presti, R. M., Paetzold, S. & Virgin, H. W. T. Latent murine cytomegalovirus infection in macrophages. *Virology* **227**, 168–179 (1997).
- Sacher, T. et al. The major virus-producing cell type during murine cytomegalovirus infection, the hepatocyte, is not the source of virus dissemination in the host. *Cell Host Microbe* **3**, 263–272 (2008).
- Brune, W., Hengel, H. & Koszinowski, U. H. A mouse model for cytomegalovirus infection. *Curr. Protoc. Immunol.* **Chapter 19**, Unit 19.17 (2001).
- Mercer, J. A., Wiley, C. A. & Spector, D. H. Pathogenesis of murine cytomegalovirus infection: identification of infected cells in the spleen during acute and latent infections. *J. Virol.* **62**, 987–997 (1988).
- Pomeroy, C., Hilleren, P. J. & Jordan, M. C. Latent murine cytomegalovirus DNA in splenic stromal cells of mice. *J. Virol.* **65**, 3330–3334 (1991).
- McNab, F., Mayer-Barber, K., Sher, A., Wack, A. & O’Garra, A. Type I interferons in infectious disease. *Nat. Rev. Immunol.* **15**, 87–103 (2015).
- Najjar, I. & Fagard, R. STAT1 and pathogens, not a friendly relationship. *Biochimie* **92**, 425–444 (2010).
- Presti, R. M., Pollock, J. L., Dal Canto, A. J., O’Guin, A. K. & Virgin, H. W. T. Interferon gamma regulates acute and latent murine cytomegalovirus infection and chronic disease of the great vessels. *J. Exp. Med.* **188**, 577–588 (1998).
- Gil, M. P. et al. Biologic consequences of Stat1-independent IFN signaling. *Proc. Natl Acad. Sci. USA* **98**, 6680–6685 (2001).
- Kropp, K. A. et al. Reversible inhibition of murine cytomegalovirus replication by gamma interferon (IFN- $\gamma$ ) in primary macrophages involves a primed type I IFN-signaling subnetwork for full establishment of an immediate-early antiviral state. *J. Virol.* **85**, 10286–10299 (2011).
- Dağ, F. et al. Reversible silencing of cytomegalovirus genomes by type I interferon governs virus latency. *PLoS Pathog.* **10**, e1003962 (2014).
- Farrell, H.E. et al. Murine cytomegalovirus spreads by dendritic cell recirculation. *mBio* **8**, e01264-17 (2017).
- Hsu, K. M., Pratt, J. R., Akers, W. J., Achilefu, S. I. & Yokoyama, W. M. Murine cytomegalovirus displays selective infection of cells within hours after systemic administration. *J. Gen. Virol.* **90**, 33–43 (2009).
- Thom, J. T., Walton, S. M., Torti, N. & Oxenius, A. Salivary gland resident APCs are Flt3L- and CCR2-independent macrophage-like cells incapable of cross-presentation. *Eur. J. Immunol.* **44**, 706–714 (2014).
- Scott, C. L. et al. The transcription factor ZEB2 is required to maintain the tissue-specific identities of macrophages. *Immunity* **49**, 312–325.e315 (2018).
- Bellomo, A. et al. Reticular fibroblasts expressing the transcription factor WT1 define a stromal niche that maintains and replenishes splenic red pulp macrophages. *Immunity* **53**, 127–142.e127 (2020).
- Spallanzani, R.G. et al. Distinct immunocyte-promoting and adipocyte-generating stromal components coordinate adipose tissue immune and metabolic tenors. *Sci. Immunol.* **4**, eaaw3658 (2019).
- Plikus, M. V. et al. Fibroblasts: origins, definitions, and functions in health and disease. *Cell* **184**, 3852–3872 (2021).
- Yamamoto, S. et al. Platelet-derived growth factor receptor regulates salivary gland morphogenesis via fibroblast growth factor expression. *J. Biol. Chem.* **283**, 23139–23149 (2008).
- Pezoldt, J. et al. Single-cell transcriptional profiling of splenic fibroblasts reveals subset-specific innate immune signatures in homeostasis and during viral infection. *Commun. Biol.* **4**, 1355 (2021).
- Mederacke, I., Dapito, D. H., Affo, S., Uchinami, H. & Schwabe, R. F. High-yield and high-purity isolation of hepatic stellate cells from normal and fibrotic mouse livers. *Nat. Protoc.* **10**, 305–315 (2015).
- Wilhelm, A. et al. CD248/endothelin critically regulates hepatic stellate cell proliferation during chronic liver injury via a PDGF-regulated mechanism. *Gut* **65**, 1175–1185 (2016).
- Buechler, M. B. et al. Cross-tissue organization of the fibroblast lineage. *Nature* **593**, 575–579 (2021).

33. Simon, C. O., Seckert, C. K., Dreis, D., Reddehase, M. J. & Grzimek, N. K. Role for tumor necrosis factor alpha in murine cytomegalovirus transcriptional reactivation in latently infected lungs. *J. Virol.* **79**, 326–340 (2005).
34. Griessl, M. et al. Stochastic episodes of latent cytomegalovirus transcription drive CD8 T-cell “memory inflation” and avoid immune evasion. *Front. Immunol.* **12**, 668885 (2021).
35. Sitnik, K. M. et al. Context-dependent development of lymphoid stroma from adult CD34(+) adventitial progenitors. *Cell Rep.* **14**, 2375–2388 (2016).
36. Oduro, J. D. et al. Murine cytomegalovirus (CMV) infection via the intranasal route offers a robust model of immunity upon mucosal CMV infection. *J. Gen. Virol.* **97**, 185–195 (2016).
37. Cardin, R. D., Schaefer, G. C., Allen, J. R., Davis-Poynter, N. J. & Farrell, H. E. The M33 chemokine receptor homolog of murine cytomegalovirus exhibits a differential tissue-specific role during in vivo replication and latency. *J. Virol.* **83**, 7590–7601 (2009).
38. Farrell, H. E. & Stevenson, P. G. Cytomegalovirus host entry and spread. *J. Gen. Virol.* **100**, 545–553 (2019).
39. Muhl, L. et al. Single-cell analysis uncovers fibroblast heterogeneity and criteria for fibroblast and mural cell identification and discrimination. *Nat. Commun.* **11**, 3953 (2020).
40. Chung, M. I., Bujnis, M., Barkauskas, C. E., Kobayashi, Y. & Hogan, B. L. M. Niche-mediated BMP/SMAD signaling regulates lung alveolar stem cell proliferation and differentiation. *Development* **145**, dev163014 (2018).
41. Tegtmeyer, P. K. et al. STING induces early IFN- $\beta$  in the liver and constrains myeloid cell-mediated dissemination of murine cytomegalovirus. *Nat. Commun.* **10**, 2830 (2019).
42. Snyder, C. M., Allan, J. E., Bonnett, E. L., Doom, C. M. & Hill, A. B. Cross-presentation of a spread-defective MCMV is sufficient to prime the majority of virus-specific CD8+ T cells. *PLoS ONE* **5**, e9681 (2010).
43. Snyder, C. M., Cho, K. S., Bonnett, E. L., Allan, J. E. & Hill, A. B. Sustained CD8+ T cell memory inflation after infection with a single-cycle cytomegalovirus. *PLoS Pathog.* **7**, e1002295 (2011).
44. Farrell, H. E., Bruce, K., Lawler, C. & Stevenson, P. G. Murine cytomegalovirus spread depends on the infected myeloid cell type. *J. Virol.* **93**, e00540-19 (2019).
45. Dupont, L. & Reeves, M. B. Cytomegalovirus latency and reactivation: recent insights into an age old problem. *Rev. Med. Virol.* **26**, 75–89 (2016).
46. Guerrero-Juarez, C. F. et al. Single-cell analysis reveals fibroblast heterogeneity and myeloid-derived adipocyte progenitors in murine skin wounds. *Nat. Commun.* **10**, 650 (2019).
47. Sinha, M. et al. Direct conversion of injury-site myeloid cells to fibroblast-like cells of granulation tissue. *Nat. Commun.* **9**, 936 (2018).
48. Reinhardt, J. W. & Breuer, C. K. Fibrocytes: A Critical Review and Practical Guide. *Front Immunol.* **12**, 784401 (2021).
49. Wallner, B. et al. Generation of mice with a conditional Stat1 null allele. *Transgenic Res.* **21**, 217–224 (2012).
50. Jordan, S. et al. Virus progeny of murine cytomegalovirus bacterial artificial chromosome pSM3fr show reduced growth in salivary glands due to a fixed mutation of MCK-2. *J. Virol.* **85**, 10346–10353 (2011).
51. Tischer, B. K., Smith, G. A. & Osterrieder, N. En passant mutagenesis: a two step markerless red recombination system. *Methods Mol. Biol.* **634**, 421–430 (2010).
52. Rand, U., Kubsch, T., Kasmapour, B. & Cicin-Sain, L. A novel triple-fluorescent HCMV strain reveals gene expression dynamics and anti-herpesviral drug mechanisms. *Front. Cell Infect. Microbiol.* **10**, 536150 (2021).
53. Kurz, S., Steffens, H. P., Mayer, A., Harris, J. R. & Reddehase, M. J. Latency versus persistence or intermittent recurrences: evidence for a latent state of murine cytomegalovirus in the lungs. *J. Virol.* **71**, 2980–2987 (1997).

## Acknowledgements

This study was funded by the Deutsche Forschungsgemeinschaft (DFG, German Research Foundation) – Projektnummer 158989968 - SFB 900; the RESIST Excellence cluster (EXC 2155, project B6); the German Centre for Infection Research (DZIF) of the German Federal Ministry of Science and Education (BMBF) through TTU 07.834 (to L.C.-S.) and the European Union’s Horizon 2020 research and innovation program under Grant Agreement 793858 (to K.M.S.). I.B. is supported by Research Coopera-bility program of the Croatian Science Foundation funded by the Eur-o-pean Union from the European Social Fund under the Operational Programme Efficient Human Resources 2014–2020 (PZS-2019-02-7879). We thank Inge Hollatz-Rangosch and Ayse Barut for technical assistance. We acknowledge Lothar Gröbe and Maria Höxter from HZI Core Flow Cytometry Facility as well as Marina Pils, Katrin Schlarman and Petra Beyer from HZI Animal Facility. We thank Mathias Müller and Birgit Strobl for providing *Stat1*<sup>-/-</sup> mice. We acknowledge Caroline Lassnig for pro-viding help with in vivo experiments. We thank Hansjörg Hauser for useful discussions.

## Author contributions

Concept and study design, K.M.S. and L.C.-S.; Investigation, K.M.S., F.K., N.G., H.M. and Y.K.; Methodology, K.M.S. and L.C.-S., Materials: U.R. and T.K.; Resources, L.C.-S. and I.B.; Funding acquisition, L.C.-S., K.M.S. and I.B.; Writing of the manuscript, K.M.S. and L.C.-S.; Supervision, K.M.S. and L.C.-S.

## Funding

Open Access funding enabled and organized by Projekt DEAL.

## Competing interests

The authors declare no competing interests.

## Additional information

**Supplementary information** The online version contains supplementary material available at <https://doi.org/10.1038/s41467-023-38449-x>.

**Correspondence** and requests for materials should be addressed to Katarzyna M. Sitnik or Luka Čičin-Šain.

**Peer review information** *Nature Communications* thanks the anon-ymous reviewer(s) for their contribution to the peer review of this work.

**Reprints and permissions information** is available at <http://www.nature.com/reprints>

**Publisher’s note** Springer Nature remains neutral with regard to jur-isdictional claims in published maps and institutional affiliations.

**Open Access** This article is licensed under a Creative Commons Attribution 4.0 International License, which permits use, sharing, adaptation, distribution and reproduction in any medium or format, as long as you give appropriate credit to the original author(s) and the source, provide a link to the Creative Commons license, and indicate if changes were made. The images or other third party material in this article are included in the article’s Creative Commons license, unless indicated otherwise in a credit line to the material. If material is not included in the article’s Creative Commons license and your intended use is not permitted by statutory regulation or exceeds the permitted use, you will need to obtain permission directly from the copyright holder. To view a copy of this license, visit <http://creativecommons.org/licenses/by/4.0/>.

© The Author(s) 2023